arXiv:hep-ex/0103012v1 11 Mar 2001

Measurement of the Branching Ratio for $\mathrm{D_s^-} \to \tau^- \bar{\nu}_\tau$ Decays

The OPAL Collaboration

Abstract

Using about 3.9 million hadronic Z decays from $\mathrm{e^+e^-}$ collisions recorded by the OPAL detector at LEP at centre-of-mass energies $\sqrt{s} \approx M_\mathrm{Z}$, the branching ratio for the decay $\mathrm{D_s^-} \to \tau^- \bar{\nu}_\tau$ has been measured to be

$$\mathrm{BR}(\mathrm{D_s^-} \to \tau^- \bar{\nu}_\tau) = (7.0 \pm 2.1(\mathrm{stat}) \pm 2.0(\mathrm{syst}))\,\%.$$

This result can be used to derive the decay constant of the $\mathrm{D_s^-}$ meson:

$$\mathrm{f_{D_s}} = (286 \pm 44(\mathrm{stat}) \pm 41(\mathrm{syst}))\,\mathrm{MeV}.$$

(submitted to Physics Letters B)

The OPAL Collaboration

G. Abbiendi[2], C. Ainsley[5], P.F. Åkesson[3], G. Alexander[22], J. Allison[16],
G. Anagnostou[1], K.J. Anderson[9], S. Arcelli[17], S. Asai[23], D. Axen[27],
G. Azuelos[18,a], I. Bailey[26], A.H. Ball[8], E. Barberio[8], R.J. Barlow[16], R.J. Batley[5],
T. Behnke[25], K.W. Bell[20], G. Bella[22], A. Bellerive[9], G. Benelli[2], S. Bethke[32],
O. Biebel[32], I.J. Bloodworth[1], O. Boeriu[10], P. Bock[11], J. Böhme[25], D. Bonacorsi[2],
M. Boutemeur[31], S. Braibant[8], L. Brigliadori[2], R.M. Brown[20], H.J. Burckhart[8],
J. Cammin[3], P. Capiluppi[2], R.K. Carnegie[6], B. Caron[28], A.A. Carter[13],
J.R. Carter[5], C.Y. Chang[17], D.G. Charlton[1,b], P.E.L. Clarke[15], E. Clay[15],
I. Cohen[22], J. Couchman[15], A. Csilling[15,i], M. Cuffiani[2], S. Dado[21],
G.M. Dallavalle[2], S. Dallison[16], A. De Roeck[8], E.A. De Wolf[8], P. Dervan[15],
K. Desch[25], B. Dienes[30,f], M.S. Dixit[7], M. Donkers[6], J. Dubbert[31], E. Duchovni[24],
G. Duckeck[31], I.P. Duerdoth[16], P.G. Estabrooks[6], E. Etzion[22], F. Fabbri[2],
M. Fanti[2], L. Feld[10], P. Ferrari[12], F. Fiedler[8], I. Fleck[10], M. Ford[5], A. Frey[8],
A. Fürtjes[8], D.I. Futyan[16], P. Gagnon[12], J.W. Gary[4], G. Gaycken[25],
C. Geich-Gimbel[3], G. Giacomelli[2], P. Giacomelli[8], D. Glenzinski[9], J. Goldberg[21],
C. Grandi[2], K. Graham[26], E. Gross[24], J. Grunhaus[22], M. Gruwé[08], P.O. Günther[3],
A. Gupta[9], C. Hajdu[29], G.G. Hanson[12], K. Harder[25], A. Harel[21], M. Harin-Dirac[4],
M. Hauschild[8], C.M. Hawkes[1], R. Hawkings[8], R.J. Hemingway[6], C. Hensel[25],
G. Herten[10], R.D. Heuer[25], J.C. Hill[5], K. Hoffman[8], R.J. Homer[1], A.K. Honma[8],
D. Horváth[29,c], K.R. Hossain[28], R. Howard[27], P. Hüntemeyer[25], P. Igo-Kemenes[11],
K. Ishii[23], A. Jawahery[17], H. Jeremie[18], C.R. Jones[5], P. Jovanovic[1], T.R. Junk[6],
N. Kanaya[23], J. Kanzaki[23], G. Karapetian[18], D. Karlen[6], V. Kartvelishvili[16],
K. Kawagoe[23], T. Kawamoto[23], R.K. Keeler[26], R.G. Kellogg[17], B.W. Kennedy[20],
D.H. Kim[19], K. Klein[11], A. Klier[24], S. Kluth[32], T. Kobayashi[23], M. Kobel[3],
T.P. Kokott[3], S. Komamiya[23], R.V. Kowalewski[26], T. Kämer[25], T. Kress[4],
P. Krieger[6], J. von Krogh[11], D. Krop[12], T. Kuhl[3], M. Kupper[24], P. Kyberd[13],
G.D. Lafferty[16], H. Landsman[21], D. Lanske[14], I. Lawson[26], J.G. Layter[4],
A. Leins[31], D. Lellouch[24], J. Letts[12], L. Levinson[24], R. Liebisch[11], J. Lillich[10],
C. Littlewood[5], A.W. Lloyd[1], S.L. Lloyd[13], F.K. Loebinger[16], G.D. Long[26],
M.J. Losty[7], J. Lu[27], J. Ludwig[10], A. Macchiolo[18], A. Macpherson[28,l], W. Mader[3],
S. Marcellini[2], T.E. Marchant[16], A.J. Martin[13], J.P. Martin[18], G. Martinez[17],
T. Mashimo[23], P. Mättig[24], W.J. McDonald[28], J. McKenna[27], T.J. McMahon[1],
R.A. McPherson[26], F. Meijers[8], P. Mendez-Lorenzo[31], W. Menges[25],
F.S. Merritt[9], H. Mes[7], A. Michelini[2], S. Mihara[23], G. Mikenberg[24], D.J. Miller[15],
W. Mohr[10], A. Montanari[2], T. Mori[23], K. Nagai[13], I. Nakamura[23], H.A. Neal[33],
R. Nisius[8], S.W. O'Neale[1], F.G. Oakham[7], F. Odorici[2], A. Oh[8], A. Okpara[11],
M.J. Oreglia[9], S. Orito[23], C. Pahl[32], G. Pásztor[8,i], J.R. Pater[16], G.N. Patrick[20],
J.E. Pilcher[9], J. Pinfold[28], D.E. Plane[8], B. Poli[2], J. Polok[8], O. Pooth[8], A. Quadt[8],
K. Rabbertz[8], C. Rembser[8], P. Renkel[24], H. Rick[4], N. Rodning[28], J.M. Roney[26],

S. Rosati[3], K. Roscoe[16], A.M. Rossi[2], Y. Rozen[21], K. Runge[10], O. Runolfsson[8],
D.R. Rust[12], K. Sachs[6], T. Saeki[23], O. Sahr[31], E.K.G. Sarkisyan[8,m], C. Sbarra[26],
A.D. Schaile[31], O. Schaile[31], P. Scharff-Hansen[8], C. Schmitt[10], M. Schröder[8],
M. Schumacher[25], C. Schwick[8], W.G. Scott[20], R. Seuster[14,g], T.G. Shears[8,j],
B.C. Shen[4], C.H. Shepherd-Themistocleous[5], P. Sherwood[15], G.P. Siroli[2],
A. Skuja[17], A.M. Smith[8], G.A. Snow[17], R. Sobie[26], S. Söldner-Rembold[10,e],
S. Spagnolo[20], F. Spano[9], M. Sproston[20], A. Stahl[3], K. Stephens[16], D. Strom[19],
R. Ströhmer[31], L. Stumpf[26], B. Surrow[8], S.D. Talbot[1], S. Tarem[21], M. Tasevsky[8],
R.J. Taylor[15], R. Teuscher[9], J. Thomas[15], M.A. Thomson[5], E. Torrence[9],
S. Towers[6], D. Toya[23], T. Trefzger[31], I. Trigger[8], Z. Trócsányi[30,f], E. Tsur[22],
M.F. Turner-Watson[1], I. Ueda[23], B. Vachon[26], C.F. Vollmer[31], P. Vannerem[10],
M. Verzocchi[8], H. Voss[8], J. Vossebeld[8], D. Waller[6], C.P. Ward[5], D.R. Ward[5],
P.M. Watkins[1], A.T. Watson[1], N.K. Watson[1], P.S. Wells[8], T. Wengler[8],
N. Wermes[3], D. Wetterling[11] J.S. White[6], G.W. Wilson[16], J.A. Wilson[1],
T.R. Wyatt[16], S. Yamashita[23], V. Zacek[18], D. Zer-Zion[8,k]

[1]School of Physics and Astronomy, University of Birmingham, Birmingham B15
2TT, UK
[2]Dipartimento di Fisica dell' Università di Bologna and INFN, I-40126 Bologna,
Italy
[3]Physikalisches Institut, Universität Bonn, D-53115 Bonn, Germany
[4]Department of Physics, University of California, Riverside CA 92521, USA
[5]Cavendish Laboratory, Cambridge CB3 0HE, UK
[6]Ottawa-Carleton Institute for Physics, Department of Physics, Carleton University, Ottawa, Ontario K1S 5B6, Canada
[7]Centre for Research in Particle Physics, Carleton University, Ottawa, Ontario
K1S 5B6, Canada
[8]CERN, European Organisation for Nuclear Research, CH-1211 Geneva 23, Switzerland
[9]Enrico Fermi Institute and Department of Physics, University of Chicago, Chicago
IL 60637, USA
[10]Fakultät für Physik, Albert Ludwigs Universität, D-79104 Freiburg, Germany
[11]Physikalisches Institut, Universität Heidelberg, D-69120 Heidelberg, Germany
[12]Indiana University, Department of Physics, Swain Hall West 117, Bloomington
IN 47405, USA
[13]Queen Mary and Westfield College, University of London, London E1 4NS, UK
[14]Technische Hochschule Aachen, III Physikalisches Institut, Sommerfeldstrasse
26-28, D-52056 Aachen, Germany
[15]University College London, London WC1E 6BT, UK
[16]Department of Physics, Schuster Laboratory, The University, Manchester M13
9PL, UK
[17]Department of Physics, University of Maryland, College Park, MD 20742, USA

[18]Laboratoire de Physique Nucléaire, Université de Montréal, Montréal, Quebec H3C 3J7, Canada

[19]University of Oregon, Department of Physics, Eugene OR 97403, USA

[20]CLRC Rutherford Appleton Laboratory, Chilton, Didcot, Oxfordshire OX11 0QX, UK

[21]Department of Physics, Technion-Israel Institute of Technology, Haifa 32000, Israel

[22]Department of Physics and Astronomy, Tel Aviv University, Tel Aviv 69978, Israel

[23]International Centre for Elementary Particle Physics and Department of Physics, University of Tokyo, Tokyo 113-0033, and Kobe University, Kobe 657-8501, Japan

[24]Particle Physics Department, Weizmann Institute of Science, Rehovot 76100, Israel

[25]Universität Hamburg/DESY, II Institut für Experimental Physik, Notkestrasse 85, D-22607 Hamburg, Germany

[26]University of Victoria, Department of Physics, P O Box 3055, Victoria BC V8W 3P6, Canada

[27]University of British Columbia, Department of Physics, Vancouver BC V6T 1Z1, Canada

[28]University of Alberta, Department of Physics, Edmonton AB T6G 2J1, Canada

[29]Research Institute for Particle and Nuclear Physics, H-1525 Budapest, P O Box 49, Hungary

[30]Institute of Nuclear Research, H-4001 Debrecen, P O Box 51, Hungary

[31]Ludwigs-Maximilians-Universität München, Sektion Physik, Am Coulombwall 1, D-85748 Garching, Germany

[32]Max-Planck-Institute für Physik, Föhring Ring 6, 80805 München, Germany

[33]Yale University,Department of Physics,New Haven, CT 06520, USA

[a] and at TRIUMF, Vancouver, Canada V6T 2A3

[b] and Royal Society University Research Fellow

[c] and Institute of Nuclear Research, Debrecen, Hungary

[e] and Heisenberg Fellow

[f] and Department of Experimental Physics, Lajos Kossuth University, Debrecen, Hungary

[g] and MPI München

[i] and Research Institute for Particle and Nuclear Physics, Budapest, Hungary

[j] now at University of Liverpool, Dept of Physics, Liverpool L69 3BX, UK

[k] and University of California, Riverside, High Energy Physics Group, CA 92521, USA

[l] and CERN, EP Div, 1211 Geneva 23

[m] and Tel Aviv University, School of Physics and Astronomy, Tel Aviv 69978, Israel.

1 Introduction

The branching ratio of the purely leptonic $D_s^- \to \ell^- \bar{\nu}_\ell$ decay[1] can be calculated [1] using

$$\mathrm{BR}(D_s^- \to \ell^- \bar{\nu}_\ell) = \frac{G_F^2}{8\pi} m_{D_s} m_\ell^2 \left(1 - \frac{m_\ell^2}{m_{D_s}^2}\right)^2 |V_{cs}|^2 \tau_{D_s} f_{D_s}^2, \tag{1}$$

where m_{D_s} is the mass and τ_{D_s} the lifetime of the D_s^- meson, f_{D_s} the D_s^- decay constant and V_{cs} the corresponding CKM matrix element. G_F denotes the Fermi coupling constant and m_ℓ the mass of the lepton.

Several models for the calculation of the decay constant f_{D_s} exist: potential models predict f_{D_s} in the range from 129 MeV to 356 MeV [1], QCD sum rule models predict $f_{D_s} = (231 \pm 24)$ MeV [2] and lattice QCD calculations predict $f_{D_s} = (240^{+30}_{-25})$ MeV [3].

The extraction of CKM matrix elements from $B^0 - \overline{B}^0$ oscillation measurements relies on these theoretical models for calculation of the decay constant for B mesons, f_B, since a measurement of f_B from $B^- \to \ell^- \bar{\nu}_\ell$ decays is currently not feasible. It is therefore important to measure f_{D_s} to test the theoretical models used in the f_B calculation. Measurements of f_{D_s} in leptonic D_s^- decays have been published by WA75 [4], BES [5], E653 [6], L3 [7], CLEO [8], and BEATRICE [9]. The measured values lie between 190 MeV and 430 MeV. The current world average is 280 ± 48 MeV [10].

In this paper, we present a measurement of $\mathrm{BR}(D_s^- \to \tau^- \bar{\nu}_\tau)$ and f_{D_s} based on reconstruction of the decay sequence

$$
\begin{aligned}
e^+ e^- \to Z \to c\bar{c} &\to D_s^{\star -} X \\
&\hookrightarrow \gamma \; D_s^- \\
&\qquad\; \hookrightarrow \tau \bar{\nu}_\tau \\
&\qquad\qquad\;\; \hookrightarrow \ell^- \bar{\nu}_\ell \nu_\tau \;\; (\ell = e, \mu).
\end{aligned}
\tag{2}
$$

Only $D_s^- \to \tau^- \bar{\nu}_\tau$ events from $Z \to c\bar{c}$ decays are considered, since a measurement of $\mathrm{BR}(D_s^- \to \tau^- \bar{\nu}_\tau)$ in $Z \to b\bar{b}$ events is systematically limited by the large uncertainty on the production rate of D_s^- mesons in $Z \to b\bar{b}$ events.

Hadronic τ decays are difficult to distinguish from background and therefore only τ decays into electrons or muons are used. Since the D_s^- mass cannot be reconstructed from a single particle in the final state, a neural network is trained on a preselected sample of hadronic Z events with one identified electron or muon, requiring the kinematics to be consistent with $D_s^- \to \tau^- \bar{\nu}_\tau \to \ell^- \bar{\nu}_\ell \nu_\tau \bar{\nu}_\tau$ decays.

In the last step of the analysis $D_s^{\star -} \to \gamma D_s^-$ decays are reconstructed in this $D_s^- \to \tau^- \bar{\nu}_\tau$ enhanced sample by forming the invariant mass of the photon and the D_s^- candidate. This reduces the dependence on the Monte Carlo simulation of the background and increases the purity of the D_s^- sample.

---

[1]Charge conjugate decays are implied throughout the paper.

Since the $D_s^- \rightarrow \ell^- \bar{\nu}_\ell$ decay is helicity suppressed, the τ channel has the largest branching ratio of all leptonic channels. Eq. 1 predicts the branching ratio into electrons to be negligible, $BR(D_s^- \rightarrow e^- \bar{\nu}_e)/BR(D_s^- \rightarrow \tau^- \bar{\nu}_\tau) < 10^{-5}$, due to the factor m_ℓ^2, whereas the branching ratio into muons, $BR(D_s^- \rightarrow \mu^- \bar{\nu}_\mu)$, is expected to be sizeable, $BR(D_s^- \rightarrow \mu^- \bar{\nu}_\mu)/BR(D_s^- \rightarrow \tau^- \bar{\nu}_\tau) = 0.103$. Therefore the decay $D_s^- \rightarrow \mu^- \bar{\nu}_\mu$ is included in the signal definition and the final result is corrected for this contribution.

2   Detector, data sample and event preselection

The OPAL detector is described in detail elsewhere [11]. Tracking of charged particles is performed by a central detector, consisting of a silicon microvertex detector, a vertex chamber, a jet chamber and z-chambers [2]. The central detector is inside a solenoid, which provides a uniform axial magnetic field of 0.435 T. The silicon microvertex detector consists of two layers of silicon strip detectors; for most of the data used in this paper, the inner layer covered a polar angle range of $|\cos\theta| < 0.83$ and the outer layer covers $|\cos\theta| < 0.77$, with an extended coverage for the data taken after the year 1996. The vertex chamber is a precision drift chamber which covers the range $|\cos\theta| < 0.95$. The jet chamber is a large-volume drift chamber, 4.0 m long and 3.7 m in diameter, providing both tracking and ionization energy loss $(\mathrm{d}E/\mathrm{d}x)$ information. The z-chambers provide a precise measurement of the z-coordinate of tracks as they leave the jet chamber in the range $|\cos\theta| < 0.72$.

The coil is surrounded by a time-of-flight counter array and a barrel lead-glass electromagnetic calorimeter with a presampler. Including the endcap electromagnetic calorimeters, the lead-glass blocks cover the range $|\cos\theta| < 0.98$. The magnet return yoke is instrumented with streamer tubes and serves as a hadron calorimeter. Outside the hadron calorimeter are muon chambers, which cover 93% of the full solid angle.

For Monte Carlo studies, event samples have been generated using JETSET 7.4 [12] for multihadronic Z events and KORALZ 4.0 [13] for τ pair events. Special signal samples have also been generated using JETSET. These consist of $Z \rightarrow c\bar{c} \rightarrow D_s^- X$ events with the decay sequence given in Eq. 2. The $D_s^- \rightarrow \tau^- \bar{\nu}_\tau$ signal is normalised using $f(c \rightarrow D_s^-) = 0.121$ [14] and $BR(D_s^- \rightarrow \tau^- \bar{\nu}_\tau) = 7.0\%$. Tau polarisation effects are handled by the τ decay library TAUOLA 2.4 [15].

The data sample used in this analysis consists of about 3.5 million Z decays recorded during the period 1991-1995 and an additional 0.4 million Z events recorded for detector calibration purposes in 1996-2000. Events are only used if the silicon microvertex detector and the other main detector components rel-

---

[2] A right handed coordinate system is used, with positive z along the e$^-$ beam direction and x pointing towards the centre of the LEP ring. The polar and azimuthal angles are denoted by θ and ϕ, and the origin is taken to be the centre of the detector.

evant for the analysis were fully operational. Hadronic Z decays are selected based on the number of reconstructed tracks and the energy deposited in the calorimeter [16]. To ensure that the event is well contained within the acceptance of the central detector, the polar angle of the thrust axis is required to satisfy $|\cos\theta_{\mathrm{T}}| < 0.8$.

Signal events are characterised by the presence of an electron or a muon from τ decays and large missing energy. Electrons and muons are identified using neural networks [17, 18] which are trained to identify leptons with a momentum greater than 2 GeV. Only events with exactly one identified electron or muon are selected. Electrons from photon conversions are rejected using a neural network conversion finder [19].

Each event is divided into two hemispheres by the plane perpendicular to the thrust axis. The hemisphere with less visible energy is required to contain the lepton. This hemisphere is selected to search for $\mathrm{D_s^-} \rightarrow \tau^- \bar{\nu}_\tau$ decays. To further enrich the sample in $c\bar{c}$ events, a loose anti-b tag [20] is applied in the hemisphere opposite to the $\mathrm{D_s^-}$. Finally, at least 9 tracks are required in an event to reduce the background from $Z \rightarrow \tau^+\tau^-$ events while keeping more than 97% of the signal events at this stage of the selection.

3 Reconstruction technique

A matching algorithm [21] is used to avoid double-counting of particle momenta in the calorimeters and in the tracking detectors. The output of the matching algorithm – referred to as particles – are tracks and calorimeter clusters.

If the missing energy in the event is only due to the neutrinos produced in the $\mathrm{D_s^-}$ decay, the energy and momentum of the $\mathrm{D_s^-}$ are exactly given by

$$\vec{P}_{\mathrm{D_s}} = - \sum_{i \neq \mathrm{lepton}} \vec{p}_i \qquad (3)$$

$$E_{\mathrm{D_s}} = \sqrt{s} - \sum_{i \neq \mathrm{lepton}} E_i \;, \qquad (4)$$

where $\sqrt{s}$ is the $\mathrm{e^+e^-}$ centre-of-mass energy. The summation is performed over all particles in the event except the lepton. The resulting mean reconstructed energy of the $\mathrm{D_s^-}$ is 27 GeV which is slightly larger than the true mean energy of 26 GeV.

Due to detector acceptance and resolution effects this method yields an energy resolution of 6.5 GeV and an angular resolution of 52 mrad where the resolution is defined as the sigma of a single Gaussian fitted to the distribution. To further improve the energy resolution, a kinematic fit is applied in which the energy and the absolute momentum of all particles (except the lepton) are varied independently from each other (i.e. varying their mass) using the constraint

6

$$\sqrt{E_{\mathrm{D_s}}^2 - P_{\mathrm{D_s}}^2} = M_{\mathrm{D_s}}. \tag{5}$$

The χ^2 values calculated from the deviations from the experimentally measured values

$$\chi^2 = \sum_{i \neq \mathrm{lepton}} \frac{(E_i^{\mathrm{fit}} - E_i^{\mathrm{meas}})^2}{\sigma_{E_i^{\mathrm{meas}}}^2} \tag{6}$$

are minimized. This procedure yields an energy resolution of about 3.0 GeV. About 2% of the events are rejected because the kinematic fit does not converge. The efficiency $\epsilon(\mathrm{D_s^-} \to \tau^- \bar{\nu}_\tau)$ to reconstruct the $\mathrm{Z} \to c\bar{c} \to \mathrm{D_s^{\star -}} X$, $\mathrm{D_s^{\star -}} \to \gamma \mathrm{D_s^-} \to \gamma \tau^- \bar{\nu}_\tau$ signal in the $\tau^- \to \mu^- \bar{\nu}_\mu \nu_\tau$ channel or in the $\tau^- \to e^- \bar{\nu}_e \nu_\tau$ channel at this stage of the analysis is about 30%.

4 Selection of $\mathrm{D_s^-} \to \tau^- \bar{\nu}_\tau$ candidates

In the next part of the analysis a $\mathrm{D_s^-} \to \tau^- \bar{\nu}_\tau$ enriched sample is selected using neural networks. About 52% of the selected events used as input to the neural networks are expected to be $\mathrm{Z} \to b\bar{b}$ events, about 36% $\mathrm{Z} \to c\bar{c}$ events and the remaining 12% Z boson decays into light quarks (uds). The signal contribution is expected to be of the order 1%. For each channel (electron or muon) two neural networks are trained: one to separate signal from $\mathrm{Z} \to c\bar{c}$ background events and one to distinguish between signal and $\mathrm{Z} \to b\bar{b}$ background.

The light-quark background is not used in the training. Since $\mathrm{D_s^-} \to \tau \nu_\tau$ decays from b decays are not considered signal, they are included in the $b\bar{b}$ background. They constitute about 0.8% of the $b\bar{b}$ background events used as input to the neural network.

The following variables are used in all four networks:

- The reconstructed energy $E_{\mathrm{D_s}}$ of the $\mathrm{D_s^-}$ obtained from the kinematic fit (Fig. 1a); the reconstruction method used for the energy and the momentum of the $\mathrm{D_s^-}$ is only valid for purely leptonic decays. Semileptonic background decays are expected to have a lower reconstructed $\mathrm{D_s^-}$ energy $E_{\mathrm{D_s}}$.

- The lepton energy E_{lep}; leptons in light-quark background events have on average lower energy than in signal events whereas leptons in background events from $b \to \ell$ decays have on average higher energy than in signal events due to the hard fragmentation of the b hadron.

- The output of two additional neural networks trained to find $b \to \ell$ (Fig. 1b) and $b \to c \to \ell$ decays [22]; leptons originating from signal events have properties more similar to leptons from $b \to \ell$ decays than from $b \to c \to \ell$ decays.

7

- The visible invariant mass determined from the tracks and clusters and the energy sum in the electromagnetic calorimeter (ECAL), both calculated in the D_s^- hemisphere; on average they are lower for signal events due to the energy carried by the neutrinos.

The choice of input variables is optimized separately for each net. The following two variables are only used in the two neural networks rejecting $b\overline{b}$ background and in the neural network separating the muon channel from the $c\overline{c}$ background:

- The momentum p_{lep,D_s} of the lepton in the D_s^- rest frame for signal events; it is limited by the mass of the D_s^- meson to be $p_{lep,D_s} < m_{D_s}/2$. The p_{lep,D_s} distribution is smeared by the experimental resolution. For leptons not originating from D_s^- decays this restriction does not exist, leading to a tail at higher p_{lep,D_s}.

- The angle between the direction of the reconstructed D_s^- and the direction of the jet containing the D_s^-; in signal events this angle is on average larger than in $Z \rightarrow q\overline{q}$ background events. The jets are reconstructed by combining all particles - including the lepton - using a cone algorithm [23]. The jet direction is then calculated excluding the lepton.

Variables sensitive to the flavour of the event are used in the neural networks separating signal from $c\overline{c}$ background:

- The highest momentum p_{max} of any particle with a charge opposite to that of the lepton in the D_s^- hemisphere (Fig. 1c); in signal events this particle should originate from the fragmentation of the c quark which produced the D_s^- meson. On average, it is therefore expected to have less momentum than the highest momentum charged particle in $c\overline{c}$ and light-quark background events.

- The angle α_{lep,D_s} between the direction of the lepton in the D_s^- rest frame and the direction of the reconstructed D_s^- in the lab frame (Fig. 1d); for $c\overline{c}$ background events the α_{lep,D_s} distribution is broad and it is peaked around $\pi/2$ while in signal events α_{lep,D_s} is closer to π.

In the neural networks which reject $b\overline{b}$ background the following variables are used:

- The number of tracks and the number of clusters in the D_s^- hemisphere; the number of clusters and the b likelihood in the opposite hemisphere.

Four selected variables which display good signal versus background separation are shown in Fig. 1. Data and background Monte Carlo distributions are in good agreement.

8

The output distributions of the neural networks for the muon channel are shown in Fig. 2. The output distributions for the electron channel are similar. In Fig. 3, two-dimensional distributions of the outputs of the neural networks are shown. A cut at 0.85 on all outputs is applied to select a $D_s^- \to \tau^- \bar{\nu}_\tau$ enriched sample with a signal efficiency of about $\epsilon(D_s^- \to \tau^- \bar{\nu}_\tau) = 9\%$.

The discrepancies between data and Monte Carlo are largest for the neural networks used to reject $Z \to c\bar{c}$ background below 0.2, far away from the cut. Discrepancies between the neural network input distributions of the data and the Monte Carlo simulation are treated as systematic uncertainties, as discussed in Section 7.

5 $D_s^{\star -}$ reconstruction

In the $D_s^- \to \tau^- \bar{\nu}_\tau$ enriched sample, events with photon candidates in the D_s^- hemisphere are used to reconstruct the decay $D_s^{\star -} \to \gamma D_s^-$. The D_s^- signal can then be observed as a peak in the $D_s^{\star -}$ mass region of the γD_s^- invariant mass distribution.

Since the neural networks have been trained to find $D_s^- \to \tau^- \bar{\nu}_\tau$ events and not specifically $D_s^{\star -} \to \gamma D_s^-$ events, additional cuts on the $D_s^- \to \tau^- \bar{\nu}_\tau$ enriched sample are required to reduce the background in the γD_s^- invariant mass distribution:

- The b likelihood as given by the b tagging algorithm [20] in the D_s^- hemisphere has to be less than 0.5 to further suppress $b\bar{b}$ background.

- Using energy and momentum conservation, the missing energy in the hemisphere is reconstructed from the visible energy $E_{\text{vis}}^{\text{hemi}}$ in the hemisphere, the invariant mass of all particles in the hemisphere, M_{hemi}, and in the opposite hemisphere, M_{opp}, via the relation:

$$E_{\text{miss}}^{\text{hemi}} = \frac{\sqrt{s}}{2} + \frac{M_{\text{hemi}}^2 - M_{\text{opp}}^2}{2\sqrt{s}} - E_{\text{vis}}^{\text{hemi}}. \tag{7}$$

  The missing energy $E_{\text{miss}}^{\text{hemi}}$ has to be larger than 15 GeV.

These two cuts reduce the efficiency for the signal to 8%.

The photon is found using information from the electromagnetic calorimeter as described in [25]. This method assigns a weight to each photon candidate corresponding to the probability for it to stem from a real photon. To accept a photon candidate, this weight has to be larger than 0.6. Only events with exactly one such photon candidate in the D_s^- hemisphere are accepted. The distribution of the photon energy E_γ after all previously defined selection cuts is shown in Fig. 4. Data and Monte Carlo simulation are in reasonable agreement. Finally, E_γ is required to be greater than 2.3 GeV. For smaller photon energies the

shapes of the invariant mass distributions of the photon and the D_s^- candidate become similar for background and signal. The energy resolution for photons with $E_\gamma > 2.3$ GeV as determined by the Monte Carlo is about 300 MeV and the angular resolution is about 5 mrad.

6 Results

The distribution of the invariant mass $m(\gamma D_s^-)$ of the photon and the D_s^- candidate for the events satisfying all selection criteria is shown in Fig. 5. In the signal region, $m(\gamma D_s^-) < 2.36$ GeV, there are 24.5 ± 2.8 background events predicted by the Monte Carlo. The number of background events is determined by requiring the expected number of Monte Carlo events to be identical to the number of data events after the lepton identification cuts described in Section 2.

The most important branching ratios have been adjusted in the Monte Carlo using the values in [10]. The uncertainty on the background is due to the limited number of Monte Carlo events. This number is subtracted from the data which yields 22.5 ± 6.9 signal events. The uncertainty is the statistical uncertainty of the data.

The efficiency to reconstruct $Z \to c\bar{c} \to D_s^{\star -} X$, $D_s^{\star -} \to \gamma D_s^- \to \gamma \tau^- \bar{\nu}_\tau$ events in the $\tau^- \to \mu^- \bar{\nu}_\mu \nu_\tau$ channel is 0.9% and in the $\tau^- \to e^- \bar{\nu}_e \nu_\tau$ channel 0.7%. If the D_s^- decays directly into muons via $D_s^- \to \mu^- \bar{\nu}_\mu$ the efficiency is 0.6%.

The branching ratio $\mathrm{BR}(D_s^- \to \tau^- \bar{\nu}_\tau)$ is extracted using

$$\mathrm{BR}(D_s^- \to \tau^- \bar{\nu}_\tau) = \frac{N_{\mathrm{cand}}}{2N_Z \cdot R_{\mathrm{C}} \cdot f(c \to D_s^-) \cdot P_V(D_s^\star, D_s) \cdot \mathrm{BR}(D_s^{\star -} \to \gamma D_s^-)}$$
$$\times \frac{1}{\mathrm{BR}(\tau \to l\bar{\nu}_l \nu_\tau) \cdot \epsilon(D_s^- \to \tau^- \bar{\nu}_\tau) + \frac{\mathrm{BR}(D_s^- \to \mu^- \bar{\nu}_\mu)}{\mathrm{BR}(D_s^- \to \tau^- \bar{\nu}_\tau)} \cdot \epsilon(D_s^- \to \mu^- \bar{\nu}_\mu)}, \tag{8}$$

where N_{cand} is the number of background-subtracted candidates in the signal region, N_Z the number of Z decays, $R_{\mathrm{c}} = 0.1671 \pm 0.0048$ [14] the partial width of the Z decaying into a pair of charm quarks, $f(c \to D_s^-) = 0.121 \pm 0.025$ [14] the production rate of D_s^- mesons in charm jets, $\epsilon(D_s^- \to \tau^- \bar{\nu}_\tau)$ the efficiency for the signal and $\epsilon(D_s^- \to \mu^- \bar{\nu}_\mu)$ the efficiency for reconstructing $D_s^{\star -} \to \gamma D_s^- \to \gamma \mu^- \bar{\nu}_\mu$ decays. As discussed in Section 1, we use $\mathrm{BR}(D_s^- \to \mu^- \bar{\nu}_\mu)/\mathrm{BR}(D_s^- \to \tau^- \bar{\nu}_\tau) = 0.103$.

$P_V(D_s^\star, D_s)$ is the ratio of $c\bar{s}$ mesons produced in a vector state $(D_s^\star)$ with respect to the sum of the pseudoscalar (D_s) and vector states. For non-strange D mesons, $P_V(D^\star, D)$ has been measured by ALEPH [26], DELPHI [27] and OPAL [28]. The averaged value is $P_V(D^\star, D) = 0.61 \pm 0.03$ [29]. To extrapolate this ratio to D_s mesons, the effect of the decays of $L = 1$ $D^{\star\star}$ resonances and quark mass effects need to be taken into account. $D^{\star\star}$ resonances contribute only in the case of non-strange mesons. This effect was estimated by OPAL to be smaller

10

than the experimental uncertainty [28] and is therefore neglected. Applying the correction factor for quark mass effects from [29] yields $P_V(D_s^\star, D_s) = 0.64 \pm 0.05$ where the full size of the correction is included in the uncertainty. This value is consistent with the ALEPH measurement of $P_V(D_s^\star, D_s) = 0.60 \pm 0.19$ [26].

Using $P_V(D_s^\star, D_s) = 0.64 \pm 0.05$ and the values given in Table 1 for the branching ratios yields

$$\mathrm{BR}(D_s^- \to \tau^- \bar{\nu}_\tau) = (7.0 \pm 2.1(\mathrm{stat}))\,\%. \tag{9}$$

7 Systematic Uncertainties

Systematic uncertainties arise from the uncertainties in the branching ratios, the Monte Carlo modelling, selection efficiencies and the detector resolution. The resulting systematic uncertainties are summarised in Table 2 and described in more detail below.

External sources: The external values used in the calculation of the branching ratios are each varied within their uncertainties.

Monte Carlo statistics The uncertainty on the background rate and on the efficiencies $\epsilon(D_s^- \to \tau^- \bar{\nu}_\tau)$ and $\epsilon(D_s^- \to \mu^- \bar{\nu}_\mu)$ due to the limited number of Monte Carlo events is counted as systematic uncertainty.

Background: To account for uncertainties in the determination of the background rate, the number of background events is also calculated using the sideband of the $m(\gamma D_s^-)$ distribution, defined by $m(\gamma D_s^-) > 2.4$ GeV. The difference between the standard analysis and the predicted background rate using the sideband is 0.1 background events in the signal region. This difference is taken as systematic uncertainty.

Background composition: About 55% of the background is due to combinations of D_s^- candidates with photons which do not originate from the same decay. The remaining background mainly consists of $D^{\star -} \to \gamma D^-$ and $D^{\star 0} \to \gamma D^0$ decays. No $D_s^- \to \tau \nu_\tau$ decays from b decays are expected in the final sample. The most important branching ratios have been varied within their uncertainties using $\mathrm{BR}(D^{\star -} \to \gamma D^-) = 0.016 \pm 0.004$, $\mathrm{BR}(D^{\star 0} \to \gamma D^0) = 0.381 \pm 0.029$, $\mathrm{BR}(D^0 \to e^- X^+) = 0.0675 \pm 0.0029$ and $\mathrm{BR}(D^0 \to \mu^- X^+) = 0.068 \pm 0.008$ [10]. The corresponding change of the result is taken as systematic uncertainty.

Fragmentation: To determine the effect of uncertainties in the Monte Carlo description of the fragmentation of b and c quarks, the distribution of the scaled hadron energy, $x_E = 2E_h/\sqrt{s}$, is reweighted within the experimental uncertainties for b quarks, $\langle x_E \rangle = 0.702 \pm 0.008$, and for c quarks, $\langle x_E \rangle = 0.484 \pm 0.008$ [14]. The largest of the variations observed using the

fragmentation functions of Peterson et al., Collins and Spiller, and Kartvel-ishvili et al. [30] is taken as systematic uncertainty.

Lepton spectrum: The exact shape of the lepton momentum spectrum for background events is not known. Therefore $b \to \ell$, $b \to c \to \ell$ and $c \to \ell$ decays are reweighted to reproduce the lepton momentum spectrum in the rest frame of the b or c hadron as predicted by the ACCMM [31], the ISGW [32] and the ISGW** [33] models. The same parameters as in [14] are used. The largest difference between the results obtained using the different models is taken as systematic uncertainty.

Tracking resolution: To take into account uncertainties in the modelling of the tracking resolution by the Monte Carlo, the reconstructed Monte Carlo track parameters are smeared by $\pm 10\%$ [24] and the analysis is repeated. The largest difference between the results is taken as an estimate for this source of systematic uncertainty.

Photon energy: The analysis is redone varying the photon energy scale in the Monte Carlo simulation by $\pm 2\%$ [25] and the difference between the results is taken as systematic uncertainty. Furthermore it was checked that the result obtained with the low purity sample in the range $1 \text{ GeV} < E_\gamma < 2.3 \text{ GeV}$ is statistically consistent with the result obtained for $E_\gamma > 2.3 \text{ GeV}$.

Lepton identification efficiency: The electron identification efficiency has been studied in [34] and has been found to be modelled correctly within 4%. The muon identification efficiency has been studied in [18], giving an uncertainty of 5%.

Neural networks: Each of the input distributions has been compared between data and Monte Carlo simulation. The simulated distributions are reweighted for each input variable in turn to agree with the corresponding data distributions, and the analysis is repeated with the weighted events. The resulting differences in the measured branching ratio are added in quadrature to obtain an estimate of the systematic uncertainty due to modelling of the input variables. This includes the uncertainty due to the Monte Carlo modelling of the missing energy $E_{\text{miss}}^{\text{hemi}}$ since some of the neural network variables are strongly correlated to $E_{\text{miss}}^{\text{hemi}}$.

b tagging: The cut on the output of the b-tag in the D_s^- hemisphere is varied in the Monte Carlo between 0.43 and 0.57 but kept at 0.5 for the data to account for uncertainties in the Monte Carlo modelling of the efficiency of the b tagging algorithm. This corresponds to a change in the b tagging efficiency of about $\pm 2\%$.

All uncertainties are added in quadrature to determine the total systematic uncertainty.

8 Conclusion

$D_s^{\star -} \to \gamma D_s^-$ decays are selected in the invariant mass distribution of the photon and the D_s^- meson. The branching ratio of D_s^- meson decays into $\tau \nu_\tau$ has been measured to be

$$BR(D_s^- \to \tau^- \bar{\nu}_\tau) = (7.0 \pm 2.1(\text{stat}) \pm 2.0(\text{syst}))\,\%,$$

in good agreement with the only other direct measurement but with a slightly smaller uncertainty [7]. From this measurement the D_s^- decay constant can be derived using Eq. 1 and the values in Table 1 to be

$$f_{D_s} = (286 \pm 44(\text{stat}) \pm 41(\text{syst}))\,\text{MeV}$$

consistent with theoretical predictions [1-3] for f_{D_s} and with the world average $f_{D_s} = 280 \pm 48$ MeV [10].

References

[1] J. Richman and P. Burchat, Rev. Mod. Phys. 67 (1995) 893, and references therein.

[2] S. Narison, Nucl. Phys. Proc. Suppl. 74 (1999) 304.

[3] T. Draper, Nucl. Phys. Proc. Suppl. 73 (1999) 43.

[4] S. Aoki et al., Prog. Theor. Phys. 89 (1993) 131.

[5] BES Collab., J.Z. Bai et al., Phys. Rev. Lett. 74 (1995) 4599.

[6] E653, K. Kodama et al., Phys. Lett. B382 (1996) 299.

[7] L3 Collab., M. Acciarri et al., Phys. Lett. B396 (1997) 327.
The measured branching ratio is $BR(D_s^- \to \tau^- \bar{\nu}_\tau) = (7.4 \pm 2.8 \pm 2.4)\%$. Using updated values from [10] and our value for $P_V(D_s^\star, D_s)$ this translates to the following decay constant: $f_{D_s} = (297 \pm 56 \pm 44)$ MeV.

[8] CLEO Collab., M. Chada et al., Phys. Rev. D58 (1998) 032002.

[9] BEATRICE Collab., V. Alexandrov et al., Phys. Lett. B478 (2000) 31.

[10] Particle Data Group, D.E. Groom et al., Eur. Phys. J. C15 (2000) 1.

[11] OPAL Collab., K. Ahmet et al., Nucl. Instr. and Meth. A305 (1991) 275;
P.P. Allport et al., Nucl. Instr. and Meth. A346 (1994) 476;
P.P. Allport et al., Nucl. Instr. and Meth. A324 (1993) 34;
O. Biebel et al., Nucl. Instr. and Meth. A323 (1992) 169;
M. Hauschild et al., Nucl. Instr. and Meth. A314 (1992) 74;
B.E. Anderson et al., IEEE Trans. Nucl. Sci. 41 (1994) 845.

[12] T. Sjöstrand, Comp. Phys. Comm. 82 (1994) 74.

[13] S. Jadach, B.F.L. Ward and Z. Was, Comp. Phys. Comm. 79 (1994) 503.

[14] The LEP Collaborations, ALEPH, DELPHI, L3 and OPAL, Nucl. Instr. and Meth. A378 (1996) 101;
updated averages are given in 'A Combination of Preliminary Electroweak Measurements and Constraints on the Standard Model', ALEPH, DELPHI, L3 and OPAL collaborations, the LEP Electroweak Working Group and the SLD Heavy Flavour and Electroweak Groups, CERN-EP-2001-xxx.

[15] S. Jadach et al., Comp. Phys. Comm. 76 (1993) 361.

[16] OPAL Collab., R. Akers et al., Z. Phys. C65 (1995) 17.

[17] OPAL Collab., G. Abbiendi et al., Eur. Phys. J. C8 (1999) 217.

[18] OPAL Collab., G. Abbiendi et al., Eur. Phys. J. C16 (2000) 41.

[19] OPAL Collab., R. Akers et al., Z. Phys. C66 (1995) 19.

[20] OPAL Collab., G. Abbiendi et al., Eur. Phys. J. C12 (2000) 567.

[21] OPAL Collab., G. Alexander et al., Phys. Lett. B377 (1996) 181.

[22] OPAL Collab., G. Abbiendi et al., Eur. Phys. J. C13 (2000) 225.

[23] OPAL Collab., R. Akers et al., Z. Phys. C63 (1994) 197.

[24] OPAL Collab., G. Abbiendi et al., Eur. Phys. J. C8 (1999) 217.

[25] OPAL Collab., G. Abbiendi et al., Eur. Phys. J. C17 (2000) 373;
OPAL Collab., K. Ackerstaff et al., Eur. Phys. J. C5 (1998) 411.

[26] ALEPH Collab., R. Barate et al., Eur. Phys. J. C16 (2000) 597.

[27] DELPHI Collab., P. Abreu et al., Eur. Phys. J. C12 (2000) 225.

[28] OPAL Collab., K. Ackerstaff et al., Eur. Phys. J. C5 (1998) 1.

[29] P.V. Chliapnikov, Phys. Lett. B470 (1999) 263.

[30] C. Peterson, D. Schlatter, I. Schmitt and P. Zerwas, Phys. Rev. D27 (1983) 105;
P. Collins and T. Spiller, J. Phys. G11 (1985) 1289;
V.G. Kartvelishvili, A.K. Likhoded and V.A. Petrov, Phys. Lett. B78 (1978) 615.

[31] G. Altarelli et al., Nucl. Phys. B208 (1982) 365.

[32] N. Isgur, D. Scora, B. Grinstein and M. Wise, Phys. Rev. D39 (1989) 799.

[33] CLEO Collab., S. Henderson et al., Phys. Rev. D45 (1992) 2212.

[34] OPAL Collab., G. Abbiendi et al., Eur. Phys. J. C8 (1999) 217.

$\mathrm{BR}(\mathrm{D_s^-} \to \tau^- \bar{\nu}_\tau)$	$f_{\mathrm{D_s}}$
$\mathrm{BR}(\mathrm{D_s^{\star-}} \to \gamma \mathrm{D_s^-}) = 0.942 \pm 0.025$ $\mathrm{BR}(\tau^- \to e^- \bar{\nu}_e \nu_\tau) = 0.1783 \pm 0.0006$ $\mathrm{BR}(\tau^- \to \mu^- \bar{\nu}_\mu \nu_\tau) = 0.1737 \pm 0.0007$	$G_{\mathrm{F}} = (1.16639 \pm 0.00001) \times 10^{-5}\,\mathrm{GeV^{-2}}$ $|V_{\mathrm{cs}}| = 0.9891 \pm 0.016$ $m_\tau = 1.77703 \pm 0.00003\,\mathrm{GeV}$ $m_{\mathrm{D_s}} = 1.9686 \pm 0.0006\,\mathrm{GeV}$ $\tau_{\mathrm{D_s}} = (0.496 \pm 0.01) \times 10^{-12}\,\mathrm{s}$

Table 1: External values used in the calculation of $\mathrm{BR}(\mathrm{D_s^-} \to \tau^- \bar{\nu}_\tau)$ and $f_{\mathrm{D_s}}$ [10].

Source	Δ BR/BR (%)
External Sources:	
$f(c \to \mathrm{D_s^-})$	20.7
$P_V(\mathrm{D_s^\star}, \mathrm{D_s})$	7.8
R_c	2.9
$\mathrm{BR}(\mathrm{D_s^{\star -}} \to \gamma \mathrm{D_s^-})$	2.7
$\mathrm{BR}(\tau^- \to \mu^- \bar{\nu}_\mu \nu_\tau)$	0.2
$\mathrm{BR}(\tau^- \to e^- \bar{\nu}_e \nu_\tau)$	0.1
Monte Carlo:	
background statistics	11.5
$\epsilon(\mathrm{D_s^-} \to \tau^- \bar{\nu}_\tau)$	2.3
$\epsilon(\mathrm{D_s^-} \to \mu^- \bar{\nu}_\mu)$	0.8
background rate	0.3
background composition	1.6
Fragmentation	1.3
Lepton spectrum	0.4
Detector resolution:	
Tracking resolution	4.7
Photon energy	6.9
Lepton identification:	
electrons	2.0
muons	4.6
Neural network inputs	8.3
b tagging	3.0
total	28.6

Table 2: Summary of relative systematic uncertainties on $\mathrm{BR}(\mathrm{D_s^-} \to \tau^- \bar{\nu}_\tau)$.
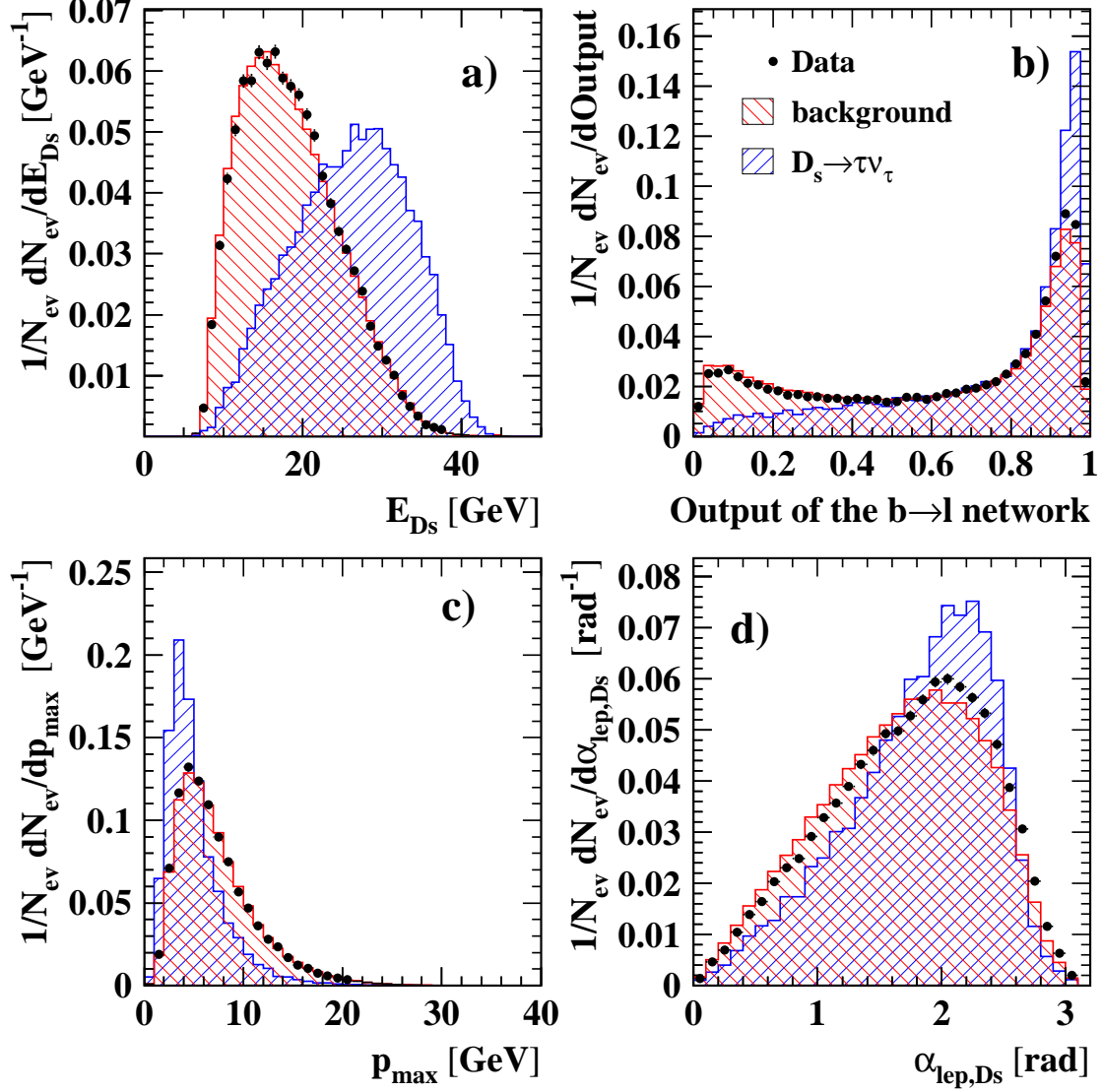
Figure 1: Four selected input variables of the neural networks used in the electron channel: a) reconstructed energy E_{D_s} of the D_s^-; b) output of the neural networks trained to find $b \to \ell$ decays; c) highest momentum p_{max} of any particle with a charge opposite to that of the lepton in the D_s^- hemisphere. d) angle α_{lep,D_s} between the lepton in the D_s^- rest frame and the D_s^-. All distributions are normalized to the number of events, N_{ev}. The signal contribution in the data is about 1% at this stage of the selection.

OPAL
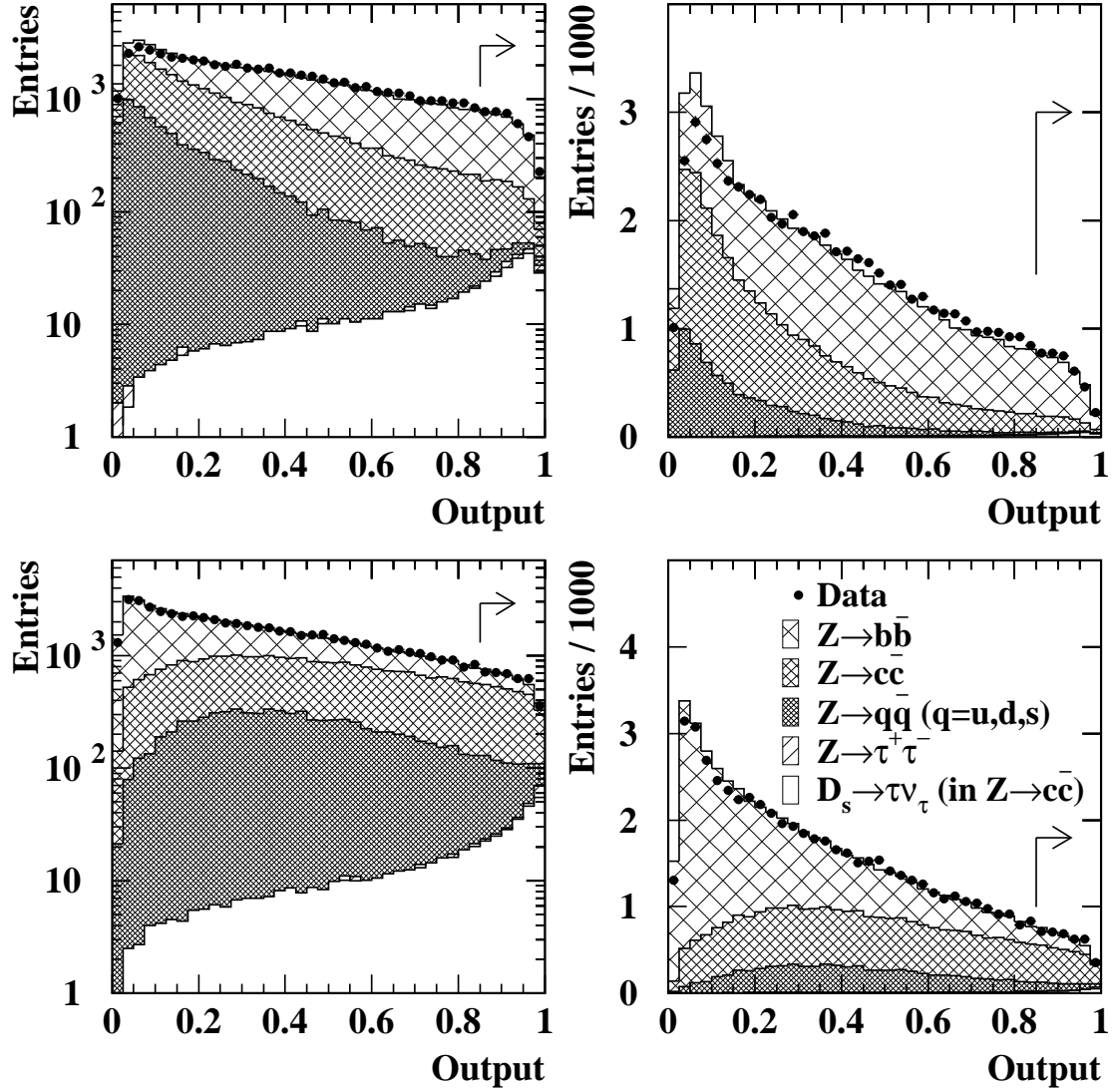
Figure 2: Muon channel: a) output of the neural network against $Z \rightarrow c\bar{c}$ background using a logarithmic scale; b) a linear scale. c) output of the neural network against $Z \rightarrow b\bar{b}$ background using a logarithmic scale; d) a linear scale. The positions of the cuts are indicated by arrows.
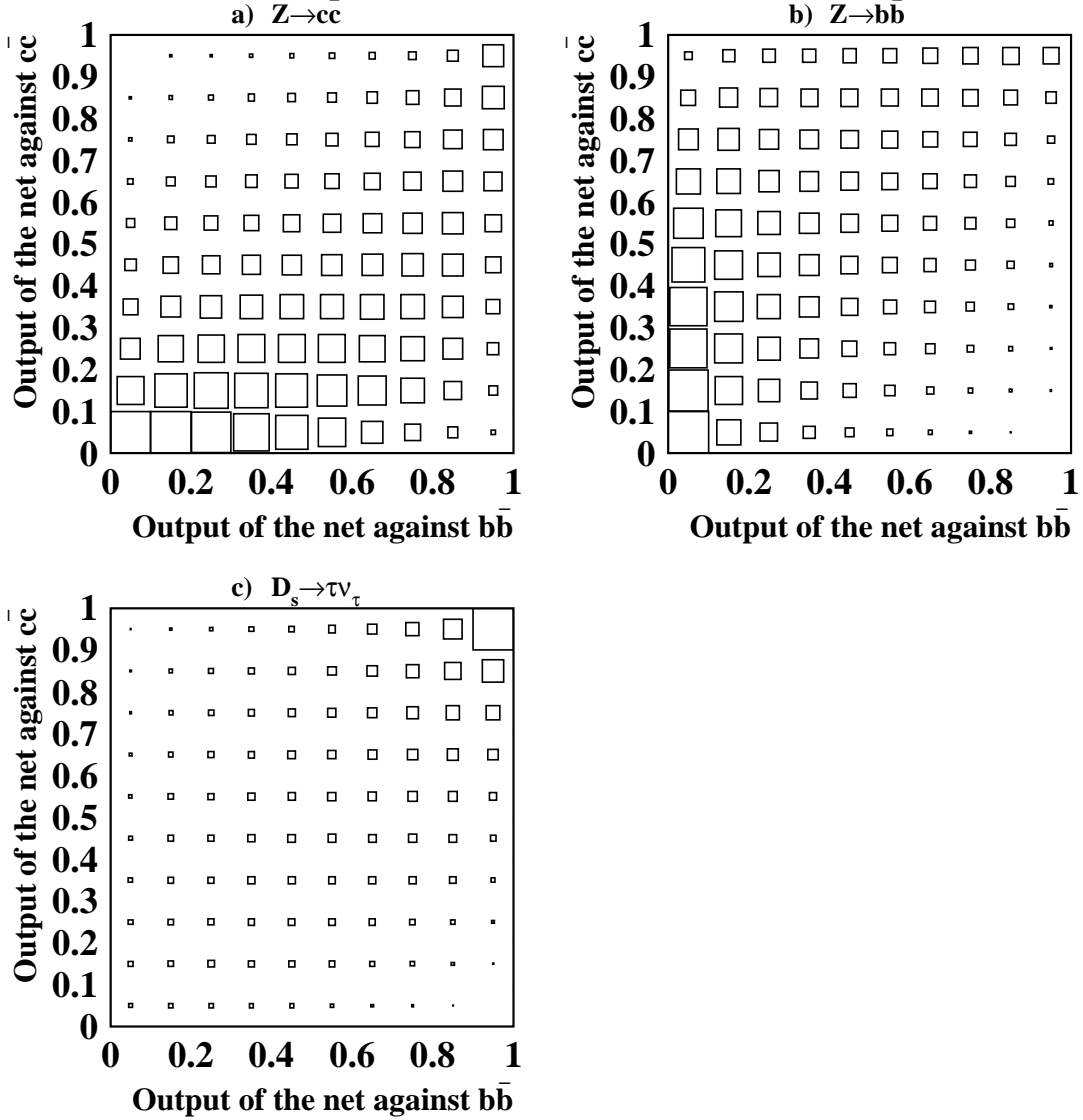
19

OPAL Monte Carlo

Figure 3: Output of the neural network against $Z \to c\bar{c}$ background events versus the output of the neural network against $Z \to b\bar{b}$ background events. The distributions for the muon and the electron channel have been added for a) $Z \to c\bar{c}$ background b) $Z \to b\bar{b}$ background and c) signal events in the Monte Carlo.

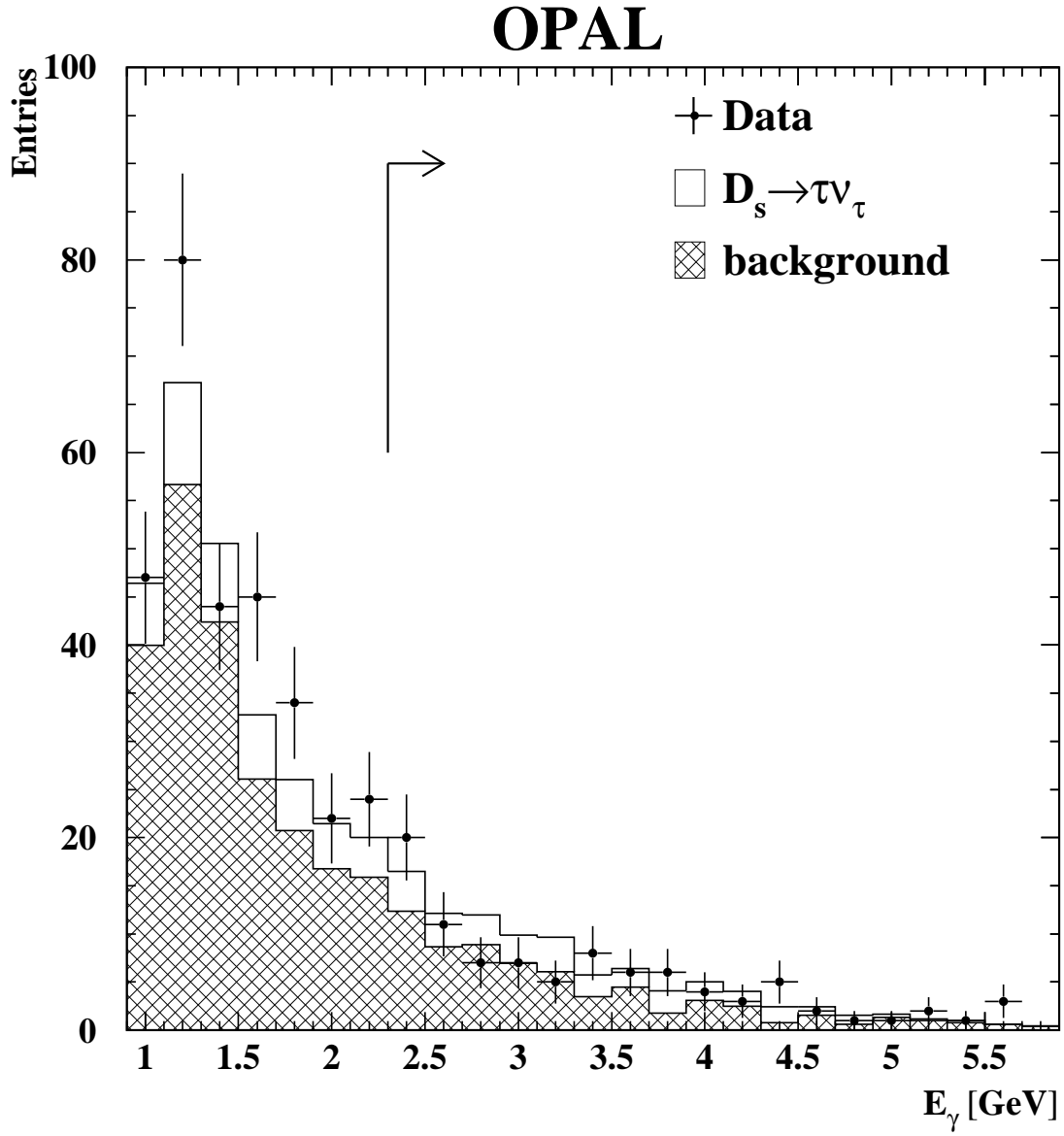Figure 4: Distribution of the photon energy E_γ for data compared to the Monte Carlo simulation. The position of the cut on E_γ is indicated by an arrow.
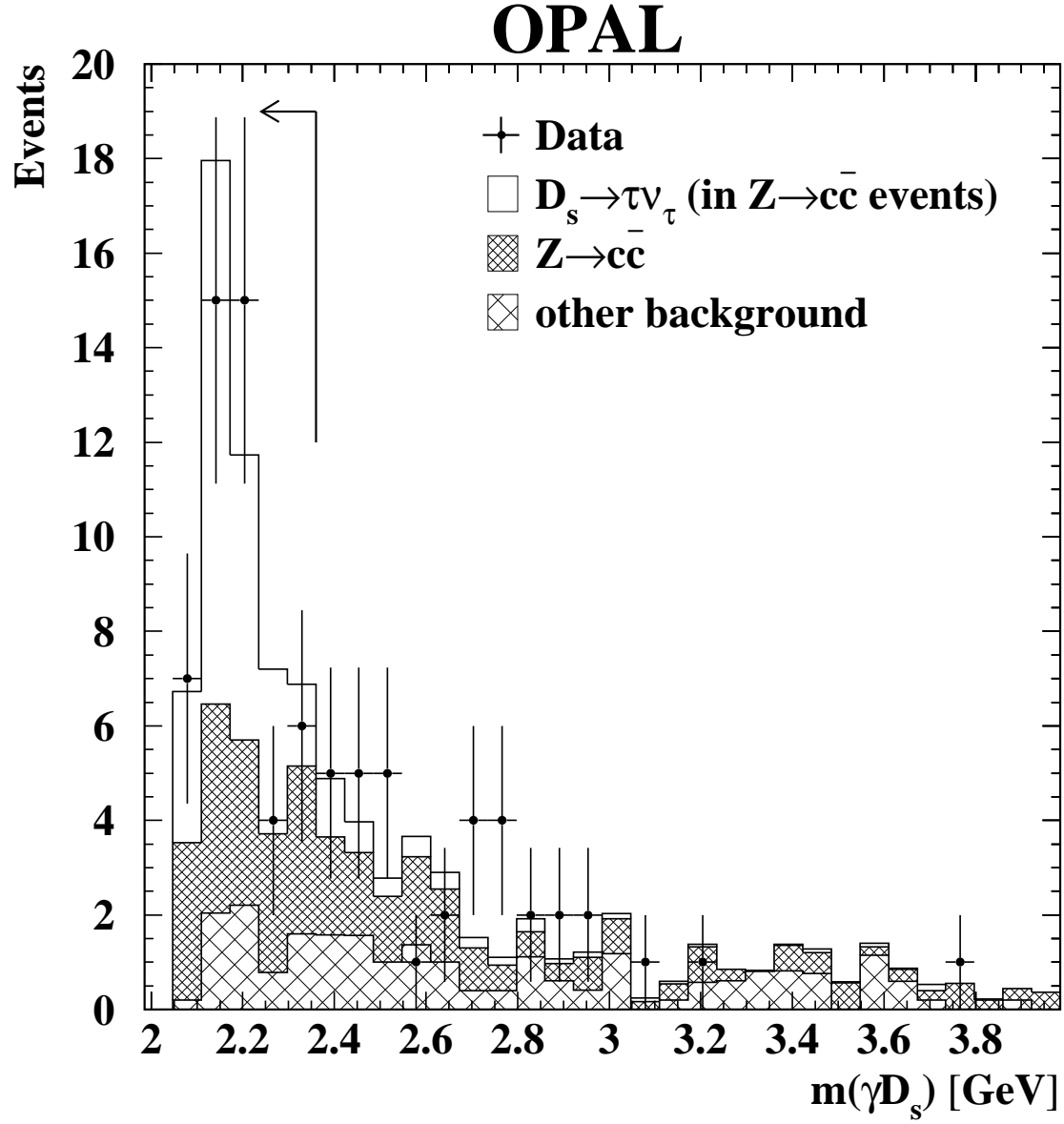
Figure 5: Invariant mass $m(\gamma D_s^-)$ of the photon and the D_s^- candidate for the events satisfying all selection criteria. The contributions to the Monte Carlo distribution from the signal and from the different sources of background are shown separately. The signal region is indicated by an arrow.